PNAS RESEARCH ARTICLE | DEVELOPMENTAL BIOLOGY OPEN ACCESS

Ablation of ZC3H11A causes early embryonic lethality and dysregulation of metabolic processes

Shady Younis[a,b,1], Alice Jouneau[c], Mårten Larsson[a], Jean-Francois Oudin[c], Pierre Adenot[c], Jihad Omar[c], Vincent Brochard[c], and Leif Andersson[a,d,1]

Contributed by Leif Andersson; received October 1, 2022; accepted May 4, 2023; reviewed by Graziano Martello and Rickard Sandberg

ZC3H11A (zinc finger CCCH domain–containing protein 11A) is a stress-induced mRNA-binding protein required for efficient growth of nuclear-replicating viruses. The cellular functions of ZC3H11A during embryonic development are unknown. Here, we report the generation and phenotypic characterization of *Zc3h11a* knockout (KO) mice. Heterozygous null *Zc3h11a* mice were born at the expected frequency without distinguishable phenotypic differences compared with wild-type mice. In contrast, homozygous null *Zc3h11a* mice were missing, indicating that *Zc3h11a* is crucial for embryonic viability and survival. *Zc3h11a* $^{-/-}$ embryos were detected at the expected Mendelian ratios up to late preimplantation stage (E4.5). However, phenotypic characterization at E6.5 revealed degeneration of *Zc3h11a* $^{-/-}$ embryos, indicating developmental defects around the time of implantation. Transcriptomic analyses documented a dysregulation of glycolysis and fatty acid metabolic pathways in *Zc3h11a*$^{-/-}$ embryos at E4.5. Proteomic analysis indicated a tight interaction between ZC3H11A and mRNA-export proteins in embryonic stem cells. CLIP-seq analysis demonstrated that ZC3H11A binds a subset of mRNA transcripts that are critical for metabolic regulation of embryonic cells. Furthermore, embryonic stem cells with an induced deletion of *Zc3h11a* display an impaired differentiation toward epiblast-like cells and impaired mitochondrial membrane potential. Altogether, the results show that ZC3H11A is participating in export and posttranscriptional regulation of selected mRNA transcripts required to maintain metabolic processes in embryonic cells. While ZC3H11A is essential for the viability of the early mouse embryo, inactivation of *Zc3h11a* expression in adult tissues using a conditional KO did not lead to obvious phenotypic defects.

ZC3H11A | mRNA export | embryonic development | RNA-binding proteins

Significance

ZC3H11A (zinc finger CCCH domain–containing protein 11A) protein has been identified as a critical factor required for the growth of human nuclear–replicating viruses. Hence, ZC3H11A is considered as a potential therapeutic target for the development of antiviral agents for medically important human viruses. This study sheds light on the cellular function of ZC3H11A during embryonic development and shows that ZC3H11A is required for early embryonic growth. Ablation of ZC3H11A is lethal in the homozygous condition and leads to complete failure of embryonic development and survival. This study reveals that ZC3H11A is critical for metabolic regulation and viability of early embryos.

The zinc finger CCCH domain–containing protein 11A (ZC3H11A) is a stress-induced messenger RNA (mRNA)-binding protein that is required for the efficient growth of several human nuclear–replicating viruses, including HIV (HIV-1), influenza A virus, human adenovirus, and herpes simplex virus 1 (1). Proteomic studies on human cells have indicated that ZC3H11A is a component of the transcription-export (TREX) complex (2). Functional studies indicated that ZC3H11A selectively exports newly transcribed viral mRNAs to the cytoplasm during viral infection (1, 3). Thereby, inactivation of ZC3H11A in human cells impaired the export of a subset of viral mRNA transcripts and resulted in a dramatic reduction in viral growth (1). These important functions of ZC3H11A in the growth cycle of several human viruses make ZC3H11A a potential target for the development of an antiviral therapy. The aim of the present study was to develop an animal model to study the molecular functions of ZC3H11A in prenatal and postnatal development.

The TREX complex serves a key function in nuclear mRNA export and consists of multiple conserved core subunits including ALYREF (RNA-binding adaptor of TREX), UAP56 (DEAD-box-type RNA helicase), and a stable subcomplex called THO, which in turn consists of at least six subunits (4, 5). Proteomic studies using human cells have indicated that ZC3H11A is an auxiliary component of the TREX complex, but did not consider it as a core subunit of the TREX complex (6, 7). THO proteins are conserved from yeast to human and play pivotal roles during embryonic development, cell differentiation, and cellular response to stimuli (8, 9). It has been reported that disruption of THO proteins, such as THOC1, THOC2, or THOC5, leads to early embryonic lethality (9–11). The TREX complex controls the mRNA export in a selective manner, where individual TREX components appear to be required for the export of distinct subsets of mRNAs (12). For instance, THOC2 or THOC5 is required for the export of mRNAs essential for pluripotency such as *Nanog*, *Sox2,* and *Klf4* in mouse embryonic stem cells (mESCs) (9). Despite several reports characterizing the role of THO proteins during embryogenesis, the cellular function of ZC3H11A during embryonic development is unknown.

Author affiliations: [a]Department of Medical Biochemistry and Microbiology, Science for Life Laboratory, Uppsala University SE-751 23, Uppsala, Sweden; [b]Division of Immunology and Rheumatology, Stanford University, Stanford, CA 94305; [c]Université Paris-Saclay, Université Saint-Quentin-en-Yvelines, Institut National de Recherche pour l'Agriculture, l'Alimentation et l'Environnement, Biologie de la Reproduction, Epigénétique, Environnement et Développement 78350, Jouy-en-Josas, France; and [d]Department of Veterinary Integrative Biosciences, Texas A&M University, College Station, TX 77843

Author contributions: S.Y. and L.A. designed research; S.Y., A.J., M.L., J.-F.O., P.A., J.O., and V.B. performed research; S.Y., A.J., and M.L. analyzed data; and S.Y., A.J., and L.A. wrote the paper.

Reviewers: G.M., Universita degli Studi di Padova; and R.S., Karolinska Institutet.

The authors declare no competing interest.

[1]To whom correspondence may be addressed. Email: syounis@stanford.edu or leif.andersson@imbim.uu.se.

This article contains supporting information online at https://www.pnas.org/lookup/suppl/doi:10.1073/pnas.2216799120/-/DCSupplemental.

Published May 30, 2023.

In the current study, we established *Zc3h11a* knockout (KO) mouse models to study the effect of *Zc3h11a* loss of function on embryonic development. Our results identify ZC3H11A as a fundamental protein required for early embryonic growth. Disruption of ZC3H11A is lethal in the homozygous condition and leads to complete failure of embryonic development and survival. Using proteomic and RNA-seq analyses, we show that the ZC3H11A protein interacts with TREX complex core proteins in mESCs. ZC3H11A is apparently an auxiliary factor participating in the export and posttranscriptional coordination of selected mRNA transcripts required to maintain the metabolic processes in embryonic cells. Interestingly, *Zc3h11a* inactivation in adult mouse tissues using an inducible mouse model showed that the ZC3H11A protein is dispensable for postnatal tissue growth.

Results

***Zc3h11a* Inactivation in Mice Is Lethal in the Homozygous Condition.** *Zc3h11a* is located on chromosome 1 in both human and mouse genomes and harbors the coding sequence of another gene encoding the DNA-binding zinc-finger protein ZBED6 (13–18) (Fig. 1*A*). We used two strategies to target the *Zc3h11a*-coding exons without affecting *Zbed6*. The first *Zc3h11a* mouse model was developed by targeting exon 3 using the CRISPR/Cas9 system with two guide RNAs flanking the targeted sequences. This resulted in both a deletion of 567 bp including the entire exon 3 and a frameshift (Fig. 1*B*). The second mouse model was developed by inserting loxP sites flanking the coding sequence of exon 2 using homologous recombination (Fig. 1*C*). These loxP mice were crossed with mice expressing Cre recombinase in germ line (PGK-Cre), which resulted in a deletion of 1.5 kb containing exon 2 and removal of the zinc-finger domains of the encoded ZC3H11A protein (Fig. 1*C*). For each model, heterozygous mice were crossed and the offspring were genotyped. No $Zc3h11a^{-/-}$ mice were obtained from heterozygous matings (Fig. 1 *D* and *E*), with the exception of one single homozygous $Zc3h11a^{-/-}$ female from the loxP mouse model (1 out of 204 mice). When we crossed this KO female with $Zc3h11a^{+/-}$ males, 10 out of 10 progeny were heterozygous $Zc3h11a^{+/-}$. The probability to get this outcome if both parents are heterozygous is $P = 0.5^{10} = 0.001$. The result confirms our interpretation that one single homozygous KO survived and was fertile.

***Zc3h11a* Deletion Results in Embryonic Degeneration.** In order to explore at what point ZC3H11A is essential for embryonic survival, we collected and genotyped embryos at different time points post $Zc3h11a^{+/-}$ X $Zc3h11a^{+/-}$ mating (Fig. 2*A*). The genotyping of embryos at embryonic day E4.5 prior to implantation revealed expected Mendelian proportions (Fig. 2*A*). However, a clear deviation from expected Mendelian proportions was observed after implantation (Fig. 2 *A*, *Bottom*). Remarkably, phenotyping at E6.5 showed dramatic changes in the morphology of the $Zc3h11a^{-/-}$ embryos with a large degree of tissue degeneration, whereas $Zc3h11a^{+/-}$ heterozygotes appeared morphologically indistinguishable from the WT embryos (Fig. 2*B*).

ZC3H11A Is Highly Expressed at the Early Stages of Embryonic Development. The lethal effect of *Zc3h11a* inactivation in mouse embryos encouraged us to explore the cellular localization of ZC3H11A at early embryonic stages. We used immunofluorescence

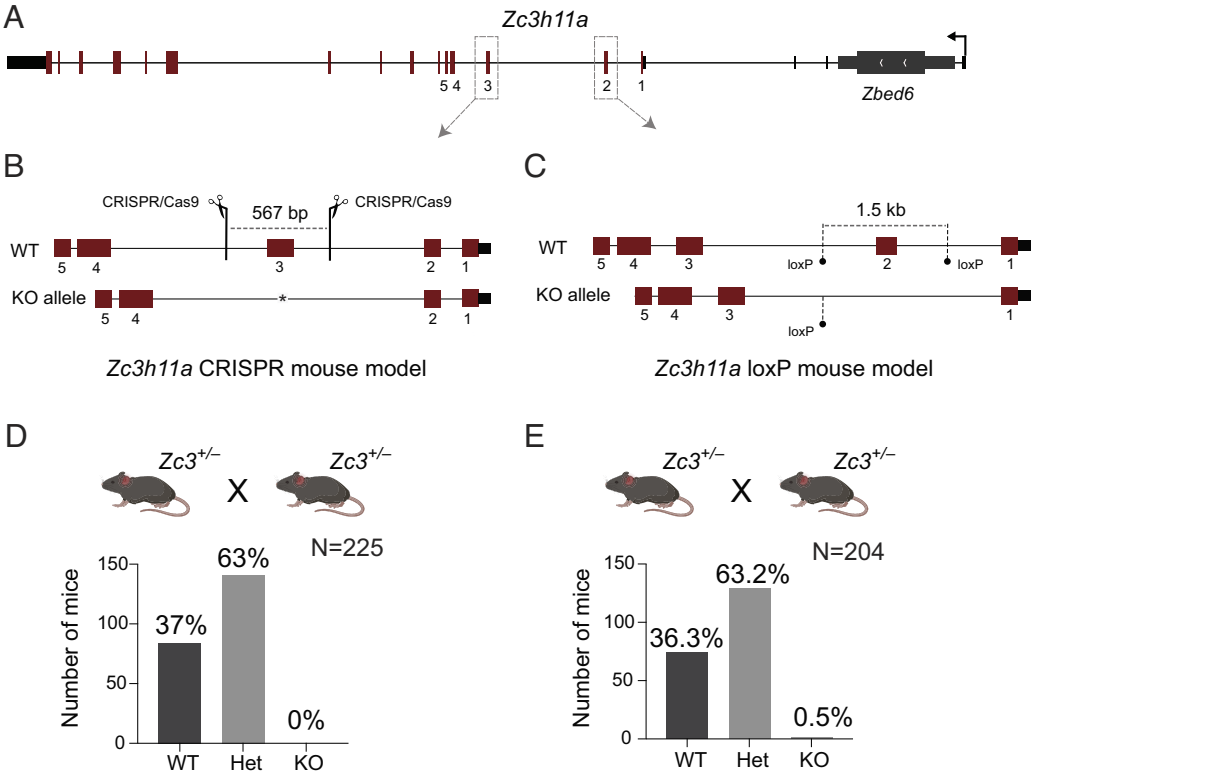

Fig. 1. Development of $Zc3h11a^{-/-}$ mouse models. (*A*) The *Zc3h11a* locus showing the targeted exons for generating $Zc3h11a^{-/-}$ mouse models. (*B*) Two CRISPR/Cas9 guide RNAs were used to delete exon 3 of *Zc3h11a*. Scissors indicate the location of the gRNAs and the length of deleted sequences. (*C*) Two homology arms were used to insert loxP sites flanking exon 2. The conditional knockout mice were crossed with mice expressing Cre in germ line to eliminate the sequences between the loxP sites, resulting in the elimination of the entire exon 2 coding sequences. (*D* and *E*) Genotyping of the offspring of *Zc3h11a* heterozygous matings ($Zc3^{+/-}$ X $Zc3^{+/-}$) using the CRISPR/Cas9-based KO mouse model (*D*) and the loxP/Cre-based KO mouse model (*E*). The total numbers of genotyped mice at week 4 are indicated.

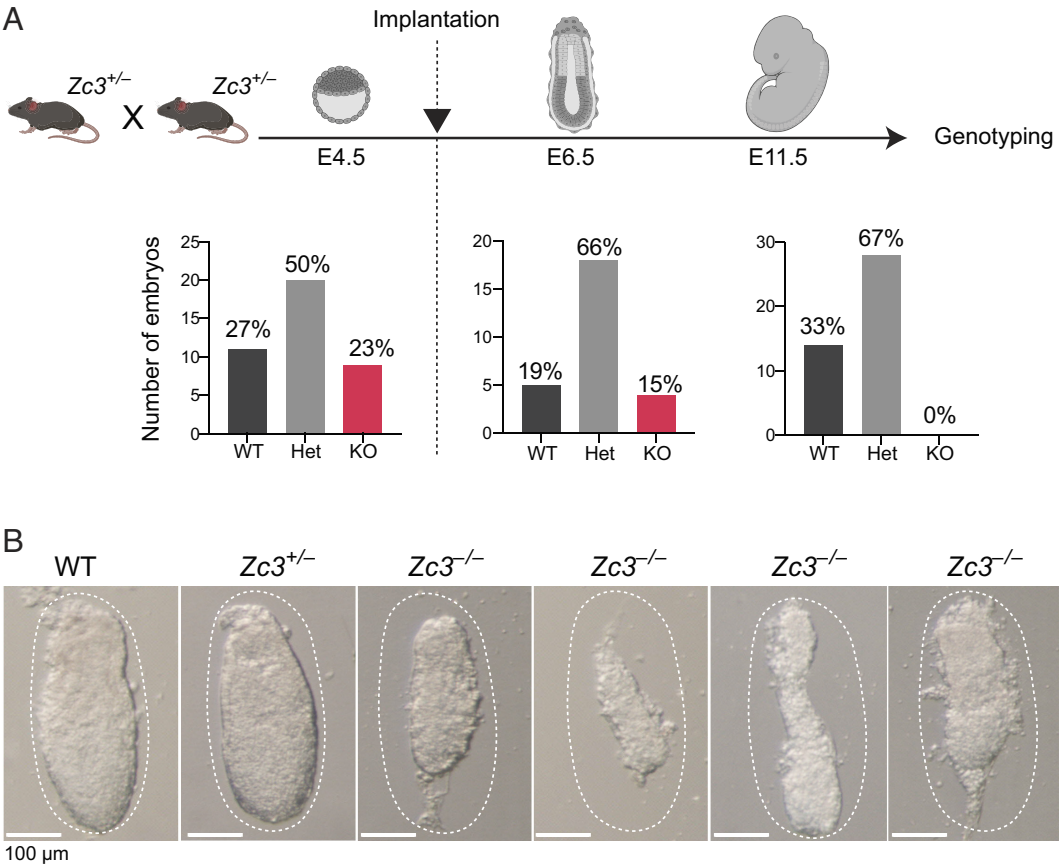

Fig. 2. Ablation of *Zc3h11a* leads to early embryonic degeneration. (*A*, *Top*) Schematic illustration showing embryonic stages and time points of collecting embryos for genotyping of *Zc3h11a*. (*A*, *Low*) Results of PCR genotyping of collected embryos at the above time points. (*B*) Morphology of collected embryos at E6.5 from *Zc3h11a* heterozygous mating ($Zc3^{+/-}$ X $Zc3^{+/-}$).

(IF) staining to visualize the ZC3H11A protein and the nuclear speckles marker SRSF2 (SC35) for expression profiling in mouse 2-cell and blastocyst stages. The IF analysis showed that ZC3H11A is expressed at a detectable level as early as the 2-cell stage, with clear nuclear localization (Fig. 3 *A*, *Top*). The z-stack imaging of the blastocysts showed that ZC3H11A was expressed in trophectoderm (TE) (Fig. 3 *A*, *Middle*) as well as in inner cell mass (ICM) (Fig. 3 *A*, *Bottom*). The localization pattern of ZC3H11A in ICM was overlapping with the nuclear speckles as indicated using the anti-SRSF2 antibody (Fig. 3 *A* and *B*). This subcellular localization of ZC3H11A in mouse embryonic cells is similar to the ZC3H11A localization in human cell lines (1). Reanalyzing single-cell RNA-seq data from Deng et al. (19) revealed that *Zc3h11a* mRNA is highly expressed in mouse embryos as early as the zygotic stage, indicating maternal contribution (Fig. 3*C*).

Disrupted Metabolic Pathways in the *Zc3h11a*$^{-/-}$ Embryos. The degeneration of *Zc3h11a* $^{-/-}$ embryos during early embryonic development (E6.5) encouraged us to perform whole-transcriptome analysis of stage E4.5 embryos to reveal the dysregulated pathways that led to the degeneration of *Zc3h11a* $^{-/-}$ embryos at E6.5. We collected embryos from $Zc3h11a^{+/-}$ X $Zc3h11a^{+/-}$ matings and extracted the RNA from the embryonic part for sequencing (Fig. 4 *A*, *Left*). Principal component analysis (PCA) of RNA-seq data showed that Het ($Zc3h11a^{+/-}$) and WT ($Zc3h11a^{+/+}$) embryos clustered together and apart from the KO ($Zc3h11a^{-/-}$) embryos (Fig. 4*A*). This result is in agreement with the observed morphological similarity between WT and Het embryos (Fig. 2*B*). Furthermore, the differential expression (DE) analysis between WT and Het did not detect any significant DE genes with FDR <0.05. Therefore, we performed the DE analysis between KO embryos vs. WT and Het embryos that revealed 660 DE genes (FDR < 0.05) out of ~11,000 expressed genes (Dataset S1). Among these DE genes, 419 were up-regulated and 241 were down-regulated in KO embryos (FDR < 0.05). Hallmark gene set enrichment analysis (GSEA) using all DE genes in KO embryos revealed a significant depletion (FDR < 0.05) of genes involved in glycolysis, fatty acid metabolism pathways, and epithelial–mesenchymal transition (EMT) processes (Fig. 4 *B*–*D*). The heatmaps present the expression of the subset of genes that contributed the most to the indicated pathway enrichment among significantly down-regulated genes in KO embryos (Fig. 4 *B*–*D*). Among the key down-regulated genes, contributing to the significant GSEA result, are lactate dehydrogenase A (*Ldha*), which has an essential role in glycolysis, and disruption of *Ldha* causes congenital disorders of carbohydrate metabolism (20, 21); enoyl-CoA hydratase and 3-hydroxyacyl CoA dehydrogenase (*Ehhadh*), which is involved in fatty acid beta-oxidation using acyl-CoA oxidase (22, 23); and dickkopf WNT signaling pathway inhibitor 1 (*Dkk1*), which is involved in several processes including cell fate determination and cell differentiation processes during embryogenesis (24). On the contrary, the positively enriched gene sets among up-regulated genes in the KO mice included genes in the P53 pathway and autophagy process–related genes (Fig. 5 *A* and *B* and *SI Appendix*, Fig. S1). This includes the upregulation of autophagy-related 12 (*Atg12*) and microtubule-associated protein 1A/1B light chain 3A (*Map1lc3a*) genes (Fig. 5*E*). MAP1LC3A is known as an LC3A protein and is required for autophagosome formation (25).

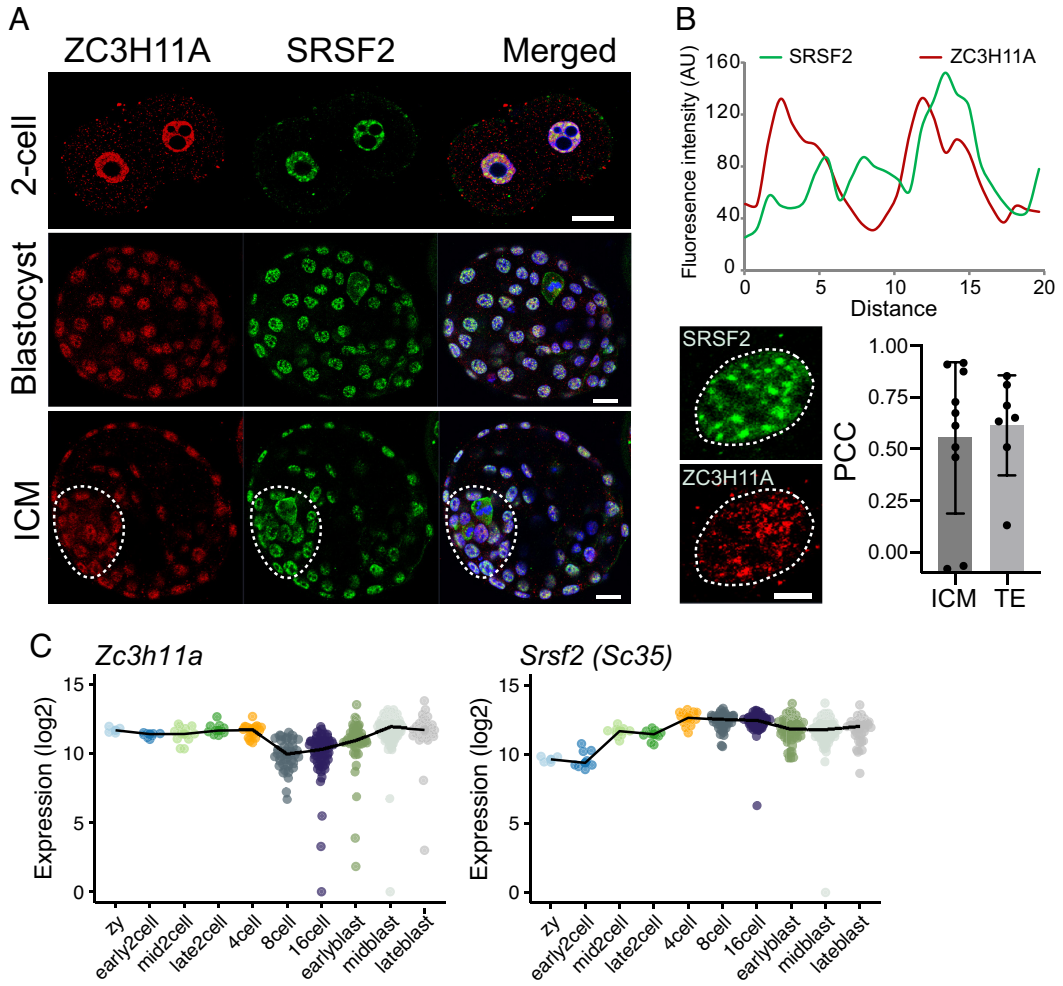

Fig. 3. Cellular localization of ZC3H11A in early embryonic cells. (*A*) Immunofluorescence staining of mouse embryos using anti-ZC3H11A and anti-SRSF2 (SC35, paraspeckle marker) antibodies at 2-cell (*Top*) and blastocyst stage (*Middle* and *Bottom*). *Middle* panel shows a z-projection of the whole blastocyst, while the *Bottom* panel is a mid-section through the ICM (scale bar: 20 μm.) (*B*) *Left*: example of a fluorescent intensity profile of ZC3H11A and SRSF2 signal across paraspeckles in an ICM nucleus showing the colocalization of ZC3H11A to paraspeckles (*Middle*, scale bar: 5 μm.). *Right*: box plots showing the distribution of the Pearson's correlation coefficients between ZC3H11A and SRSF2 profiles across several paraspeckles. (*C*) Expression of *Zc3h11a* and *Srsf2* measured by smartseq2 single-cell RNA-seq. Reanalysis of data from Deng et al. (19).

To get further insight on which cell type in blastocysts was most affected by *Zc3h11a* inactivation, we explored the expression profile of the DE genes in *Zc3h11a*$^{-/-}$ embryos in embryonic lineages (ICM and epiblast) and TE. Using previously published datasets of mouse gene expression [GSE76505 (26)], the ICM/TE ratio of expression was computed for genes down-regulated and up-regulated in the KO embryos (FDR ≤ 0.05, fold change ≥ 2). We also explored the expression of DE genes at earlier stages using gene expression dataset (E-MTAB-2950) (27). This showed that down-regulated genes in *Zc3h11a*$^{-/-}$ embryos are primarily expressed in the ICM/early epiblast rather than TE (Fig. 5*C*), while the expression of the up-regulated genes is nearly equally present in ICM/early epiblast and TE (*SI Appendix*, Fig. S2). The down-regulated genes in *Zc3h11a*$^{-/-}$ embryos with high expression in the ICM include *Ldha,* teratocarcinoma-derived growth factor 1 (*Tdgf1* alias *Cripto)*, growth differentiation factor 3 (*Gjb3*), and phosphofructokinase (*Pfkp*) (Fig. 5*D*). GDF3 is an analog of NODAL and uses TDGF1 as a cofactor (28). *Ldha*, *Pfkp, Pfkm,* and *Pdk2* are down-regulated in *Zc3h11a*$^{-/-}$ embryos and are involved in glycolysis and lactate production, as indicated in the GSEA (Fig. 4). At periimplantation stages, there is a major metabolic switch from oxidative phosphorylation to anaerobic glycolysis, with increased lactate production (29, 30). *Tdgf1* has been reported as an essential factor regulating this metabolic switch (31). This provides a plausible explanation for the finding that the down-regulated pathways revealed by the GSEA results mostly concern metabolic regulation processes. Altogether, this strongly suggests that the primary consequence of ZC3H11A deficiency is in the ICM, due to perturbed metabolic regulation. The enrichment of genes associated with autophagy and apoptosis-related pathways (Fig. 5 *A* and *B*) among the up-regulated genes in *Zc3h11a*$^{-/-}$ embryos could be a secondary effect caused by the metabolic stress encountered by the ICM cells (32, 33).

ZC3H11A Is Associated with the RNA Export Machinery in Embryonic Stem Cells. In human somatic cells, ZC3H11A has been recently characterized as an RNA-export protein that functions through its interaction with TREX complex proteins (1). In order to identify its interacting partners in embryonic cells and to investigate whether ZC3H11A maintains its association with the TREX complex in mESCs, we performed co-immunoprecipitations (co-IPs) using anti-ZC3H11A, anti-THOC2, and anti-IgG antibodies followed by mass spectrometry (MS) analyses (Fig. 6*A*). Statistical analyses of detected MS intensities from the biological replicates (n = 4) revealed a number of proteins with statistically significant interaction with ZC3H11A

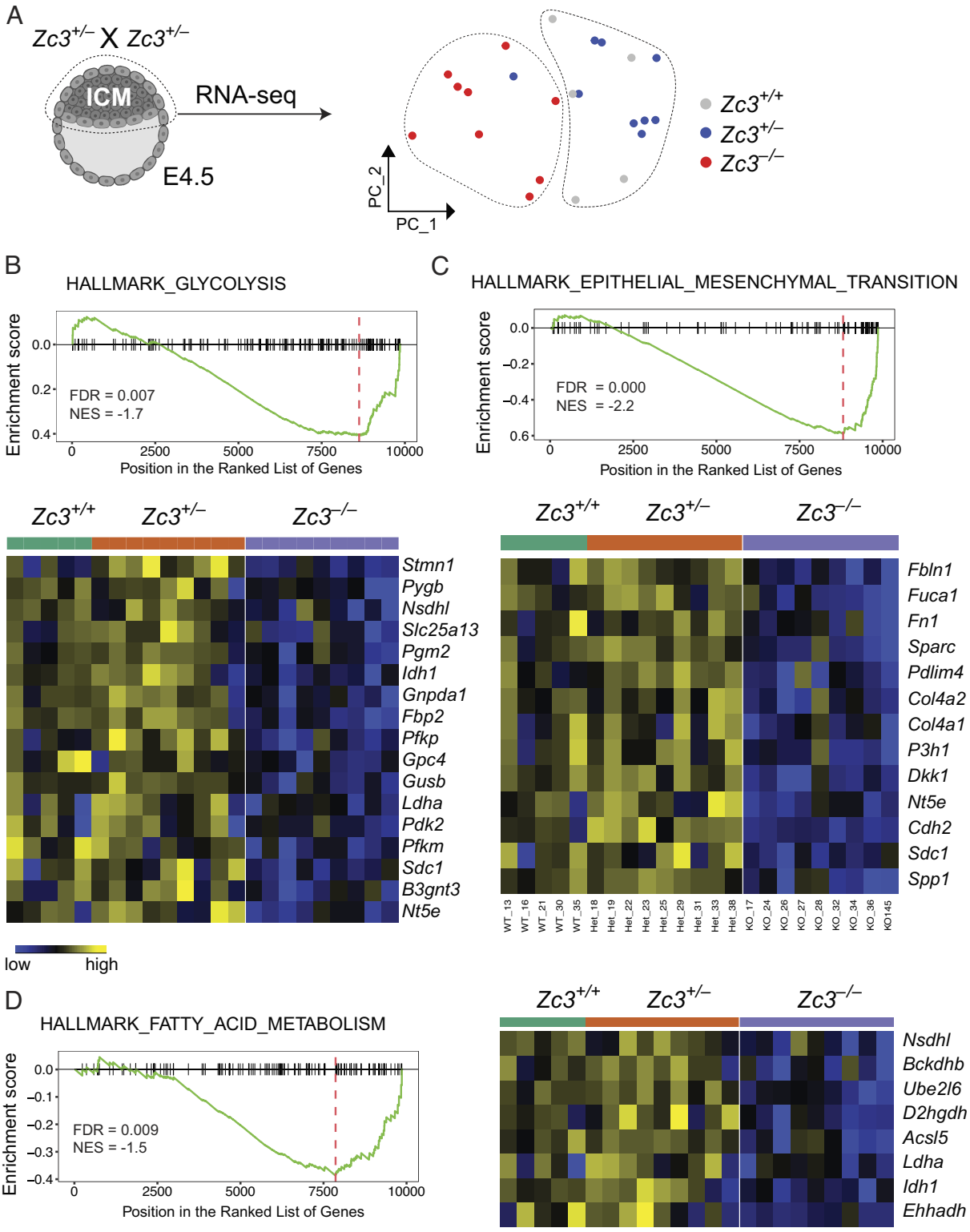

Fig. 4. Transcriptome analysis reveals dysregulated pathways in *Zc3h11a*$^{-/-}$ embryos. (*A*, *Left*) Dissected inner cell mass (ICM) cells were used for RNA-sequencing. (*A*, *Right*) Principal component analysis (PCA) of RNA-seq data from embryonic parts at E4.5. Dots represent individual embryos and colors represent different genotypes. (*B–D*) Gene set enrichment analysis (GSEA) of ranked DE genes in *Zc3h11a*$^{-/-}$ embryos using hallmark gene sets. (*B* and *C*, below) Heatmaps showing the expression of the genes contributing to the above pathways and found significantly down-regulated in *Zc3h11a*$^{-/-}$ embryos (FDR < 0.05). (*D*) Heatmap showing the expression of the genes contributing to fatty acid metabolism pathway and found significantly down-regulated in *Zc3h11a*$^{-/-}$ embryos (FDR < 0.05). FDR: false discovery rate, NES: normalized enrichment score.

and THOC2 (Fig. 6*B*). Proteins belonging to the TREX complex and RNA-export machinery are highlighted in bold. The log-fold change in protein intensities in the ZC3H11A co-IP relative to the IgG co-IP is presented along with the adjusted *P*-values (Fig. 6*C*). The interaction between ZC3H11A and THOC2 was validated by a reciprocal co-IP and western blot using mESCs (Fig. 6*D*). The majority of the significant partners interacting with ZC3H11A are part of the TREX complex and also showed

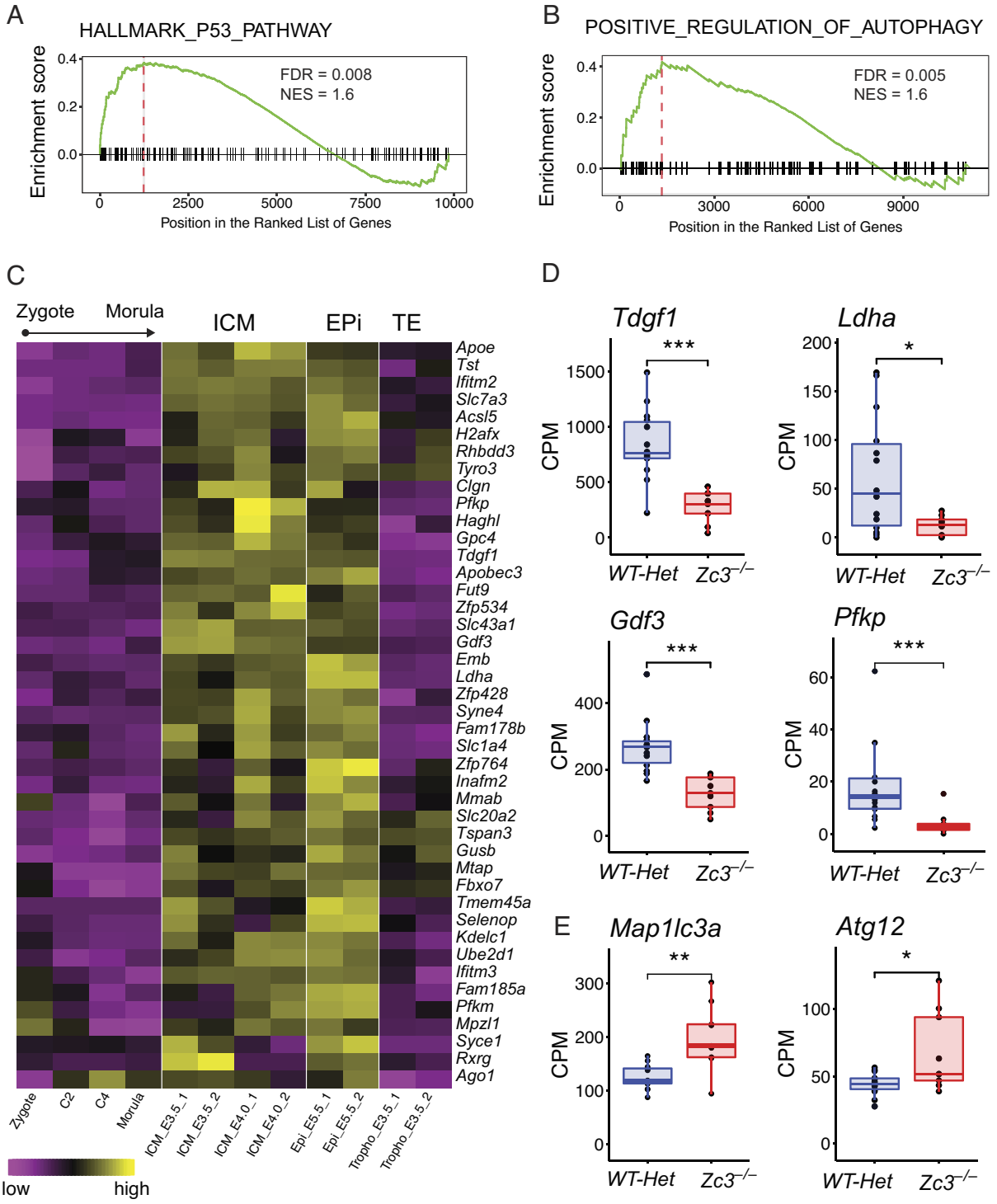

Fig. 5. Down-regulated genes in *Zc3h11a*$^{-/-}$ embryos are ICM related. (*A* and *B*) GSEA of ranked genes in *Zc3h11a*$^{-/-}$ embryos with positive enrichment for the P53 pathway (*A*) and autophagy-related genes (*B*) among the up-regulated genes in *Zc3h11a*$^{-/-}$ embryos. (*C*) Heatmap of down-regulated genes in *Zc3h11a*$^{-/-}$ embryos (FDR < 0.05) and their expression profile during embryonic stages as indicated. Reanalyzed data from GSE76505 and E-MTAB-2950. (*D* and *E*) Expression level of the indicated genes as counts per millions. *, **, and *** correspond to *FDR*< 0.05, 0.01, and 0.001, respectively.

significant enrichment in the THOC2 co-IP, including THOC5, THOC7 (Fig. 6*E*), THOC1, and THOC6 (Fig. 6*C*). ZC3H11A also interacts with other RNA-binding proteins that are required for RNA maturation, such as polyadenylate-binding nuclear protein 1 (PABPN1) (34); FYTTD1, which acts as an adaptor for RNA helicase UAP56 (35); and the RNA export adaptor ALYREF/THOC4 (36) (Fig. 6 *D* and *F*). Notably, almost half of the ZC3H11A partners detected by co-IP were also found in the THOC2 co-IP (*SI Appendix*, Fig. S3). These data indicate that ZC3H11A is an essential component of the TREX complex that is known to play pivotal roles during embryogenesis and for maintaining pluripotency of ESCs (9, 10). Furthermore, the proteomic analysis identified additional interacting partners, independent of the TREX complex, such as the RNA-binding protein DDX18; the polycomb repressive complex 2 components SUZ12 and JARID2; and the two zinc-finger proteins ZNF638

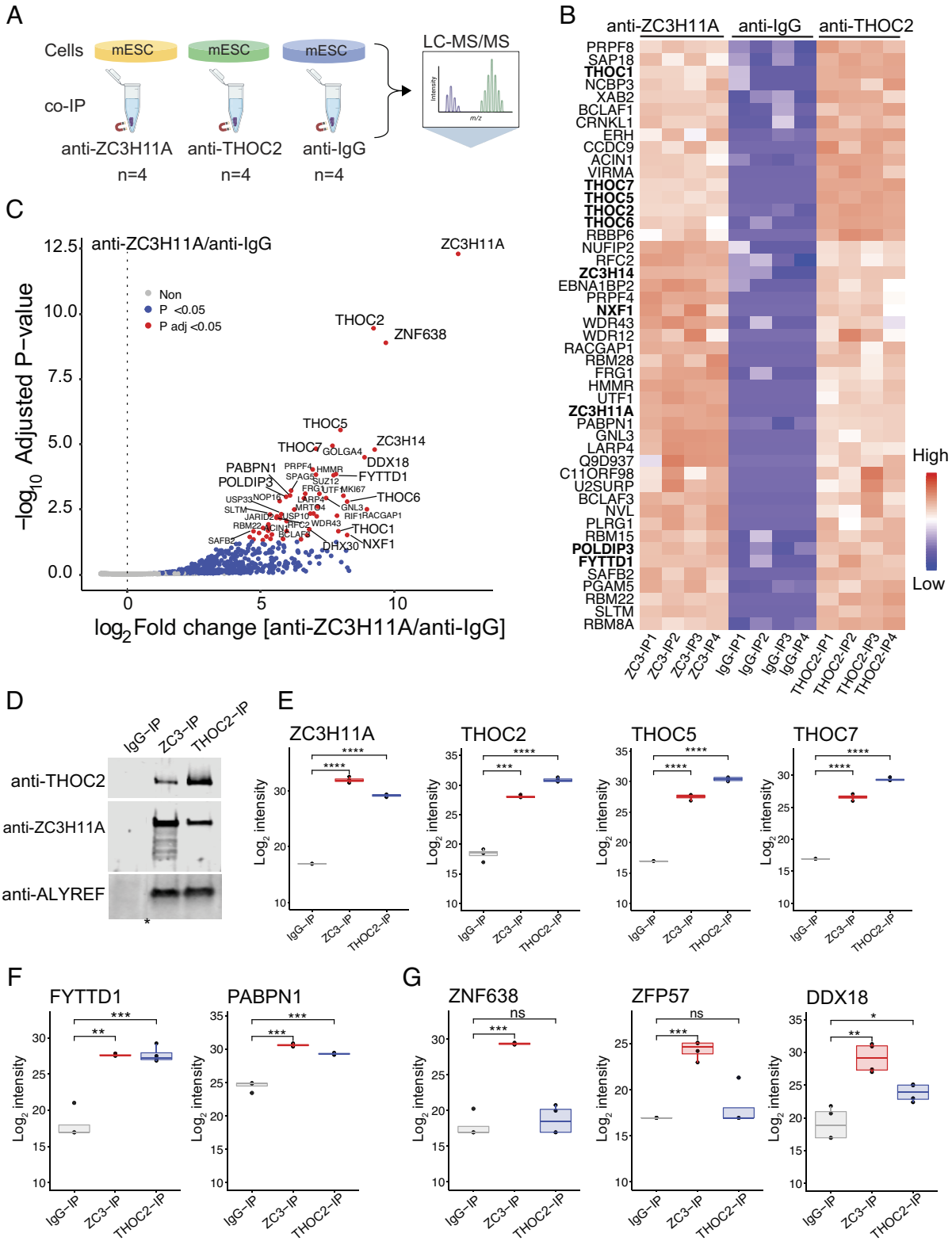

Fig. 6. ZC3H11A binds RNA-export TREX complex proteins in mESC. (*A*) Schematic illustration of co-immunoprecipitation (co-IP) mass-spectrometry experiments using anti-ZC3H11A, anti-THOC2, and anti-IgG antibodies and mouse embryonic stem cells (mESCs). (*B*) Heatmap of the interacting partners to ZC3H11A (adjusted $P < 0.05$). Data presented as log intensities of four replicates. Proteins associated with the TREX-complex and mRNA export are in bold. (*C*) Volcano plot showing the enrichment of co-IP proteins from anti-ZC3H11A/anti-IgG. (*D*) Western blot of reciprocal co-IP using anti-ZC3H11A, anti-THOC2, and anti-IgG antibodies and probed with the indicated antibodies. Asterisk indicates a cut in the western blot membrane. (*E*) Log intensities of the ZC3H11A and THOC proteins. (*F*) Log intensities of FYTTD1 (UAP56) and the polyadenylation factor PABPN1. (*G*) Log intensities of proteins interacting with ZC3H11A independent of THOC2 and the TREX complex. *, **, ***, and **** correspond to adjusted $P < 0.05$, 0.01, 0.001, and 0.0001, respectively. ns: not significant.

and ZFP57 (Fig. 6*G* and *SI Appendix*, Fig. S3*B*). DDX18 is an RNA-binding protein that plays a crucial role in pluripotency and self-renewal of embryonic stem cells (37).

ZC3H11A Selectively Binds mRNA Transcripts in mESCs. Previous studies using human somatic cells indicated that ZC3H11A is an RNA-binding protein that selectively binds subsets of mRNA upon stress or viral infection (1). To study the RNA-binding properties of ZC3H11A in embryonic cells, we performed UV-cross-linking of mESCs followed by ZC3H11A immunoprecipitation (CLIP) and RNaseI treatment to isolate the RNA protected by ZC3H11A. We used two anti-ZC3H11A antibodies to minimize any artifact caused by antibodies, and anti-ALYREF and anti-IgG as positive and negative controls, respectively. High-throughput sequencing of the RNA isolated by CLIP (CLIP-seq) revealed an almost exclusive interaction between ZC3H11A and protein-coding mRNAs in mESCs (*SI Appendix*, Fig. S4*A* and Fig. 7*A*); the much higher number of peaks at 3′UTRs compared with 5′UTRs can be explained by the longer length of the former. The analysis of ZC3H11A CLIP-seq peaks from the two ZC3H11A antibodies revealed a significant enrichment of short purine-rich motifs (Fig. 7 *B*, *Top*). Moreover, ZC3H11A exhibited strong binding to the paraspeckle *Neat1* transcript (*SI Appendix*, Fig. S4*B*), similar to what has been observed in human somatic cells (1). Comparing the CLIP-seq ZC3H11A mRNA targets with genes that were significantly down-regulated in RNA-seq data, we identified subsets of genes as putative direct targets of ZC3H11A in mESCs (Fig. 7 *B*, *Bottom*). The gene ontology analysis of these genes suggested that they are involved in germ cell development and metabolic processes (Fig. 7*C*). These 29 genes were dramatically

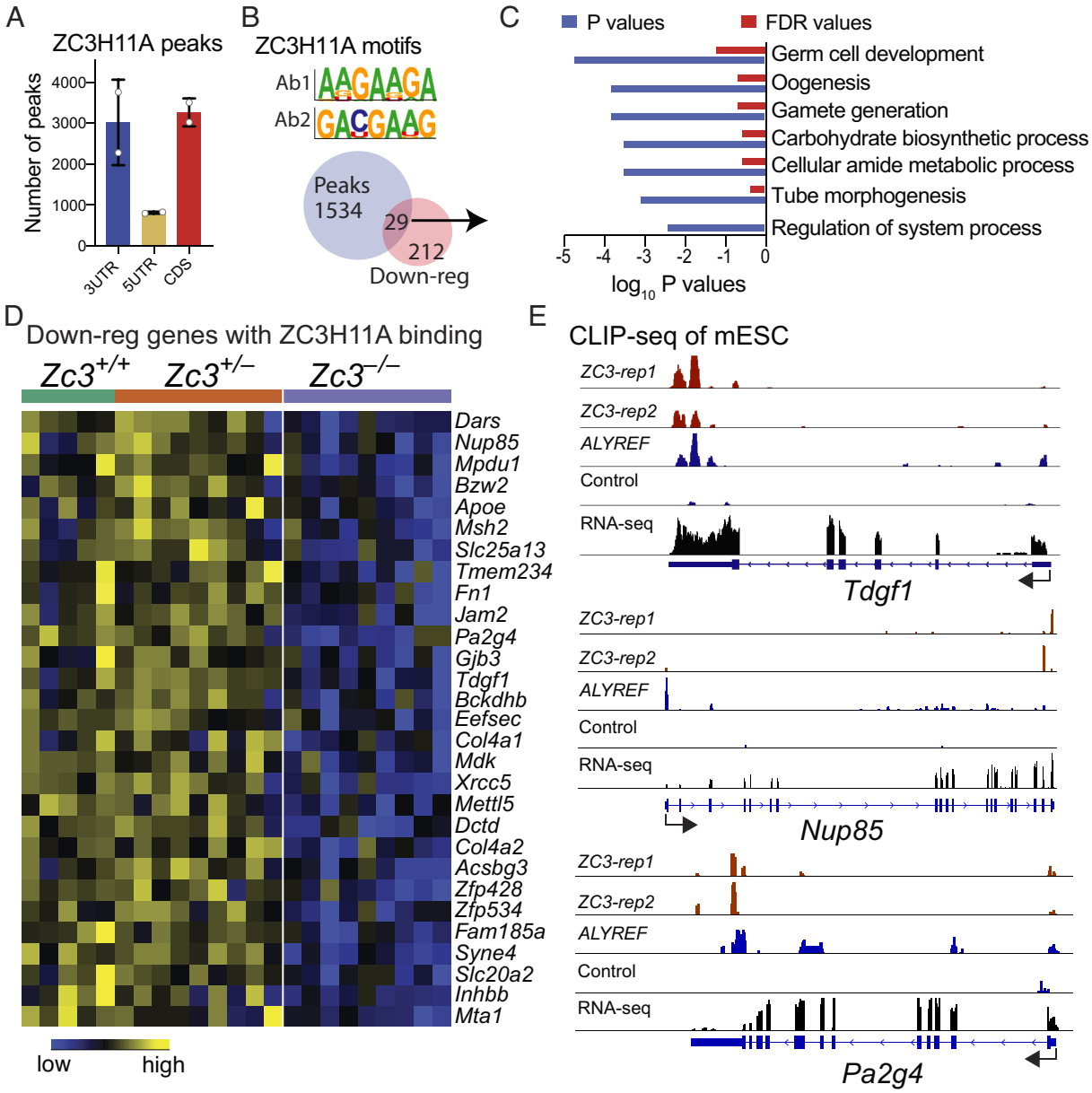

Fig. 7. CLIP-seq analysis of ZC3H11A RNA targets in mESCs. (*A*) Distribution of the proportion of ZC3H11A CLIP-seq–mapped reads over the various elements of a gene in mESC using two anti-ZC3H11A antibodies and an anti-IgG control antibody. (*B*, *Top*) Predicted motifs for ZC3H11A binding. (*B*, *Bottom*) The overlap between differential down-regulated genes in KO embryos and predicted ZC3H11A CLIP-seq targets. (*C*) Gene ontology analysis of the down-regulated genes with ZC3H11A-binding sites. (*D*) Heatmap of the down-regulated genes with ZC3H11A-binding sites. (*E*) The visualization of CLIP-seq reads and their distribution over the indicated genes. Black arrows indicate the direction of transcription from 5′ UTR to 3′ UTR.

down-regulated in *Zc3h11a*$^{-/-}$ embryos (Fig. 7*D*) and are involved in cellular processes vital for embryonic development (38–41). Putative direct targets included the *Tdgf1,* nucleoporin 85 (*Nup85*), proliferation-associated protein 2G4 (*Pa2g4*), and gap junction protein beta 3 genes (*Gjb3*). The CLIP-seq analysis detected ZC3H11A-binding sites at the 3'UTR of these genes that either overlapped with ALYREF-binding sites (for *Tdgf1* and *Pa2g4*) or did not (*Nup85*) (Fig. 7*E*). These results suggest a crucial role of ZC3H11A in posttranscriptional processing and mRNA export of key genes in embryonic cells.

ZC3H11A Is Required for In Vitro Derivation of ESCs. To further understand the role of ZC3H11A in the periimplantation development and especially its role in the pluripotent epiblast, twenty-five E3.5 blastocysts were recovered from matings between heterozygous mice, and cultured in vitro. From these, 14 ESC lines were obtained but none were homozygous KO (X^2= 4.7, d.f. = 1; $P < 0.05$). This suggests that ZC3H11A is required for establishing ESC in vitro.

Mice with Postnatal *Zc3h11a* Ablation Are Healthy and Viable. We developed an inducible *Zc3h11a*-KO model to assess the effect of *Zc3h11a* ablation postnatally. LoxP-*Zc3h11a* mice were crossed with mice containing fusion of a mutated estrogen receptor T2 and Cre recombinase (Cre-ER), allowing temporal control of floxed gene deletion upon tamoxifen induction in vivo (42). We generated a strain that is homozygous *Zc3h11a*-loxP ($Zc3^{loxP/loxP}$) with one copy of Cre-ER (CRE.ER$^+$ $Zc3^{loxP/loxP}$) and crossed it with the original strain ($Zc3^{loxP/loxP}$) lacking Cre-ER. The offspring were injected with tamoxifen at weeks 3 to 4 after birth (Fig. 8*A*). Genotyping of the tamoxifen-injected mice at week 6 using genomic DNA from tail biopsies revealed a balanced ratio between WT and induced KO (iKO) due to the presence/absence of Cre-ER (Fig. 8*B*). By injecting CRE.ER$^+$ $Zc3^{loxP/loxP}$ mice with tamoxifen postnatally, we succeeded in achieving >90% reduction of *Zc3h11a* expression in multiple adult tissues including bone marrow, liver, and spleen (Fig. 8 *C* and *D*). The examination of tamoxifen-injected mice was carried out at week 12 and involved histology staining of multiple organs including stomach, pancreas, and small and large intestine tissues. The histology phenotyping did not exhibit obvious defects between the floxed (WT) and iKO adult mice (Fig. 8*E* and *SI Appendix*, Fig. S5). Furthermore, the measurement of body weight and the weight of dissected kidney and spleen tissues from WT and inducible ZC3-KO adult mice did not show significant differences (Fig. 8*F*).

Impaired Differentiation and Metabolism in *Zc3h11a*-Induced Ablation in ESCs. After treatment with tamoxifen, iKO ESCs did not show any mortality or growth defect and maintained pluripotency as shown by RT-qPCR analysis (*SI Appendix*, Fig. S6*A*). This shows that ZC3H11A is not required for ESC maintenance, once they are established, in agreement with the Mendelian recovery of blastocysts. In vivo, the defects occur at the periimplantation stages, corresponding to a change in pluripotency from a naïve to a primed state (43). To mimic this evolution, we converted ESCs into primed epiblast-like cells (EpiSCs), by transferring them to a medium containing FGF2 and activin A. During such in vitro conversion, a higher cell loss was observed for iKO cells than that for floxed controls (*SI Appendix*, Fig. S6*B*) and the iKO EpiSCs colonies were less compact and smaller than WT (*SI Appendix*, Fig. S6*C*). Genotyping performed on cDNA confirmed the absence of WT cells among the iKO population (*SI Appendix*, Fig. S6*D*). The expected changes in gene markers of the naïve and primed pluripotency states were observed for both types of cells (*SI Appendix*, Fig. S6*E*). Although not statistically significant, *Ldha* and *Tdgf1* were slightly down-regulated in iKO cells at day 4. We then assessed changes in mitochondrial activity in the naïve state (ESCs) and after 2 d of conversion. For that, we used a sensitive live reporter of mitochondrial membrane potential, the carboyanine dye JC-1. It allowed the simultaneous detection of monomer forms (green fluorescence) at low mitochondrial potential and aggregates (red fluorescence) formed at high potential (Fig. 8*G*). Interestingly, we observed that iKO cells have a lower ratio of aggregates/monomers at both time points, suggesting an impaired energy metabolism in the absence of *Zc3h11a* (Fig. 8*H*). These results are in line with the defective metabolism of in vivo developed KO embryos, as deduced from RNA-seq data.

Discussion

ZC3H11A is important for the growth of nuclear-replicating viruses, where viruses take advantage of the ZC3H11A protein to facilitate the export of their mRNA transcripts into cytoplasm. Thereby, ZC3H11A is considered a possible target for the development of antiviral therapy. Hence, we developed ZC3H11A mouse models to study their physiological functions across developmental stages. The current study reports that ZC3H11A is an essential protein required for the viability of mouse embryos. Loss of function of ZC3H11A leads to developmental defects and embryonic degeneration at periimplantation stages associated with the dysregulation of metabolic pathways such as glycolysis and fatty acid metabolic processes. Interestingly, the defects mainly originate from the epiblast, as most of the down-regulated genes are expressed predominantly in this lineage. Moreover, even though ZC3H11A is expressed in all cells of the blastocyst, *Tdgf1*, one of its key down-regulated target genes, is expressed specifically in the epiblast cells (31). TDGF1 (also called Cripto) is a membrane-bound protein, a coreceptor for NODAL/GDF3 (44). TDGF1 and NODAL signaling plays important roles during specification of the early lineages and maintenance of the pluripotent epiblast at early postimplantation stages (44). Interestingly, it also controls the metabolic switch occurring at the time of implantation in the mouse, when cells transit from an OXPHOS-based metabolism to a glycolytic one (29, 31, 45). Our CLIP-seq analysis detected two strong peaks for ZC3H11A binding at the 3′ end of the *Tdgf1* mRNA in mESCs (Fig. 7*E*). Furthermore, ZC3H11A binds the 3′ end of the *Nup85* and *Pa2g4* mRNA transcripts (Fig. 7*E*). Both *Nup85* and *Pa2g4* were down-regulated in the KO embryos and play crucial roles in embryonic development (38–41). For instance, NUP85 is a core component of the nuclear pore complex (NPC) proteins and is required for mRNA export and maintenance and assembly of the NPC (40, 41, 46). Loss-of-function studies showed that inactivation of the NPC proteins in mouse models resulted in early embryonic lethality (47–49). Recent phenotypic characterization of the *Nup85* KO mouse model from the International Mouse Phenotyping Consortium (www.mousephenotype.org, accessed August 22, 2022) (50) has indicated complete preweaning lethality of *Nup85*$^{-/-}$ mice. Furthermore, the ErbB3-binding protein-1 gene (*Ebp1*/*Pa2g4*) is implicated in regulating the proliferation and differentiation during developmental stages. The *Pa2g4* KO mice exhibited growth retardation and were 30% smaller than wild-type mice (51). A recent study has reported more severe phenotypes in *Pa2g4*-deficient mice with death between E13.5 and 15.5, massive apoptosis, and cessation of cell proliferation (38). These

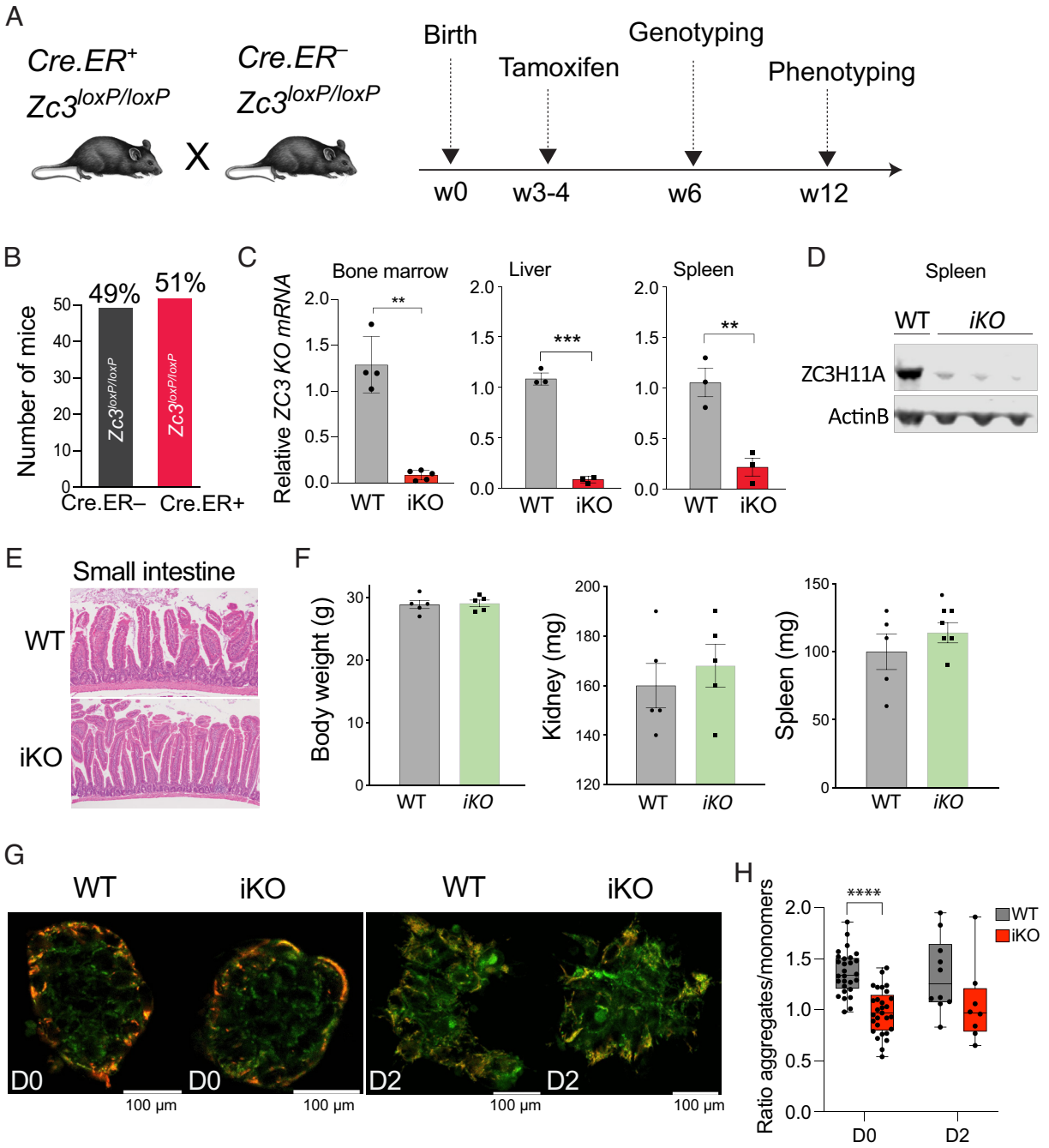

Fig. 8. Phenotype characterization of conditional *Zc3h11a*-KO mice and ESCs. (*A*) The loxP-*Zc3h11a* mouse model was crossed with mice containing a fusion of a mutated estrogen receptor and Cre recombinase (Cre-ER). The mice were bred to obtain two genotypes of homozygous loxP-*Zc3h11a* mice ($Zc3^{loxP/loxP}$): one with one copy of Cre-ER ($CRE.ER^{+}$ $Zc3^{loxP/loxP}$) and the other with null Cre-ER ($CRE.ER^{-}$ $Zc3^{loxP/loxP}$). These mice were crossed and the offspring were injected with tamoxifen at weeks 3 to 4 after birth. The time line indicates the time points of injection and sample collection for genotyping and phenotyping. (*B*) Genotyping of the Cre-ER $Zc3^{loxP}$ mice. (*C*) qPCR analysis of *Zc3h11a* mRNA expression in the bone marrow, liver, and spleen tissues from WT and induced Zc3-KO (iKO) mice both injected with tamoxifen. ** and *** correspond to *t*-test $P < 0.01$ and 0.001, respectively. (*D*) Western blot analysis of spleen tissues dissected from WT and iKO adult mice. (*E*) Histology (H&E staining) of the small intestine from WT and induced iKO adult mice. (*F*) Body weight in grams (g) and weight of dissected kidney and spleen in milligrams (mg) from WT and induced iKO adult mice. Results are means ± SEM. (*G*) Fluorescence imaging of the mitochondrial membrane potential reporter JC-1 in WT and iKO ESCs before (D0) and after 2 d of in vitro conversion toward epiblast-like stage. Aggregates formed under high potential appear red, while monomers (low potential) are green. (*H*) Boxplots showing ratios of aggregates to monomers in WT and iKO at D0 and D2 of conversion. **** corresponds to Wilcoxon rank-sum test, $P < 0.0001$.

putative ZC3H11A targets identified by CLIP-seq are known to be critical for embryonic viability and implicated in diverse cellular functions, and disruption of their expression leads to embryonic degeneration.

Another key down-regulated gene in KO embryos is *Ldha*, the enzyme that controls the level of anaerobic glycolysis by catalyzing the transformation of pyruvate into lactate. Hence, in KO embryos, the establishment of a more anaerobic glycolysis is impaired, which compromises survival when the environment becomes more hypoxic as embryos implant. Upregulation of autophagy as observed in KO embryos can be viewed as a reaction to a suboptimal metabolic environment (33). Although KO embryos can survive up to E6.5, they have already undergone a process of degeneration, as suggested by the upregulation of P53-mediated apoptotic pathway already at E4.5. The transcriptomic analysis also indicated a significant dysregulation in the EMT process (Fig. 4*C*). The EMT process is fundamental for

embryonic development and takes place during implantation of the embryo into the uterus and during early gastrulation, where embryo is transformed from a single layer to three germ layers. Defects in EMT and subsequently in gastrulation usually lead to a failure in embryonic development (52, 53).

The ZC3H11A protein exhibited strong interactions with members of the RNA-export machinery in ESCs, and the top interacting partners with ZC3H11A are members of the TREX complex, including THO proteins (Fig. 6). The enrichment analysis of interacting partners with ZC3H11A showed significant enrichment of proteins involved in the metabolism of RNA, mRNA 3′-end processing, and transport of mature transcript to cytoplasm (*SI Appendix*, Fig. S3*A*). These proteomics results are in agreement with the analysis of the CLIP-seq of ZC3H1A in mESCs that revealed an almost exclusive interaction between ZC3H11A and protein-coding mRNAs (Fig. 7*A*). It also supports the model of action that ZC3H11A interacts with TREX-complex proteins and contributes to efficient mRNA maturation and export of the target transcripts. In agreement with this model, several studies have described the pivotal roles of the TREX-complex in the embryonic development (9–11). THO proteins such as THOC1, THOC2, and THOC5 play essential roles during early development but in a different way than ZC3H11A, as their depletion affects pluripotency establishment and maintenance (9, 10). In contrast, ZC3H11A depletion does not directly affect pluripotency maintenance. The fact that *Zc3h11a*$^{-/-}$ blastocysts did not give rise to ESC lines in the present study may be due to the metabolic impairment rather than a defect in pluripotency maintenance, as they all form outgrowth, in contrast to *Thoc1*$^{-/-}$ embryos (10). This is further demonstrated by the impaired mitochondrial membrane potential after inactivation of *Zc3h11a* in ESCs.

Our results provide evidence that ZC3H11A is required for the posttranscriptional regulation of genes that are crucial for the embryonic cell. In contrast to the severe phenotypes in *Zc3h11a* germline KO embryos, *Zc3h11a* inactivation in the adult tissues did not cause obvious defects. The phenotypic characterization of the inducible ZC3-KO adult mice indicated a dispensable role for ZC3H11A in adult tissues, and a single surviving *Zc3h11a*$^{-/-}$ female showed no pathological conditions, was fertile, and gave birth to 10 progeny from three litters. Furthermore, complete inactivation of *Zc3h11a* in human and mouse cell lines did not lead to significant effects on cell growth or viability (1, 3).

Methods

Detailed descriptions on how we developed *Zc3h11a*$^{-/-}$ mice; performed RNA sequencing, protein characterization, MS, CLIP-seq analysis, and bioinformatic analysis; and developed and characterized embryonic stem cells can be found in *SI Appendix*.

Ethics Statement

Animal procedures were carried out according to the rules and regulations of the Swedish Animal Welfare Agency and French national rules on Ethics and Animal Welfare in the Animal Facility; and were in compliance with the European Communities Council Directive of 22 September 2010 (2010/63/EU). This work was approved by the French Ministry of Higher Education, Research, and Innovation (no. 15-55 &21-01) and the local Ethical Committee (INRAE Jouy-en-Josas Centre). The study was carried out in compliance with the ARRIVE guidelines.

Data, Materials, and Software Availability. The MS proteomics data (Fig. 6 and *SI Appendix*, Fig. S3) have been deposited to the ProteomeXchange Consortium (http://proteomecentral.proteomexchange.org) (54) via the MassIVE partner repository (http://massive.ucsd.edu) with the accession numbers MSV000091811 (https://massive.ucsd.edu/ProteoSAFe/dataset.jsp?accession=MSV000091811) and PXD041852 (https://proteomecentral.proteomexchange.org/cgi/GetDataset?ID=PXD041852). The RNA-seq reads have been submitted to the sequence read archive (http://www.ncbi.nlm.nih.gov/sra) with the accession number PRJNA961171.

ACKNOWLEDGMENTS. This project was funded by the Swedish Research Council (2017-02907) and the Knut and Alice Wallenberg Foundation (KAW 2017.0071), as well as by the French REVIVE Labex (Investissement d'Avenir, ANR-10-LABX-73). S.Y. is the recipient of an European Molecular Biology Organization short-term fellowship (STF-8256). J.O. is the recipient of REVIVE and INRAe PHASE department fellowships. Sequencing was performed by the SNP&SEQ Technology Platform in Uppsala. The Swedish facility is part of the National Genomics Infrastructure Sweden and Science for Life Laboratory. The SNP&SEQ Platform is also supported by the Swedish Research Council and the Knut and Alice Wallenberg Foundation. Animal experiments performed in France were done in INRAE Infectiology of Fishes and Rodents Facility (IERP-UE907, Jouy-en-Josas Research Center), which belongs to the National Distributed Research Infrastructure for the Control of Animal and Zoonotic Emerging Infectious Diseases through In Vivo Investigation (EMERG'IN, doi: 10.15454/1.5572352821559333E12). Fluorescent images were acquired in the French ISC MIMA2 (Microscopy and Imaging Facility for Microbes, Animals and Foods, doi: 10.15454/1.5572348210007727E12).

1. S. Younis *et al.*, Multiple nuclear-replicating viruses require the stress-induced protein ZC3H11A for efficient growth. *Proc. Natl. Acad. Sci. U.S.A.* **115**, E3808–E3816 (2018).
2. E. G. Folco, C.-S. Lee, K. Dufu, T. Yamazaki, R. Reed, The proteins PDIP3 and ZC11A associate with the human TREX complex in an ATP-dependent manner and function in mRNA export. *PLoS One* **7**, e43804 (2012).
3. L. Yang *et al.*, Porcine ZC3H11A is essential for the proliferation of pseudorabies virus and porcine Circovirus 2. *ACS Infect. Dis.* **8**, 1179–1190 (2022).
4. C. G. Heath, N. Viphakone, S. A. Wilson, *The Role of TREX in Gene Expression and Disease* (Portland Press Ltd, 2016).
5. B. Chi *et al.*, Aly and THO are required for assembly of the human TREX complex and association of TREX components with the spliced mRNA. *Nucleic Acids Res.* **41**, 1294–1306 (2013).
6. K. Dufu *et al.*, ATP is required for interactions between UAP56 and two conserved mRNA export proteins, Aly and CIP29, to assemble the TREX complex. *Genes Dev.* **24**, 2043–2053 (2010).
7. M. Y. Hein *et al.*, A human interactome in three quantitative dimensions organized by stoichiometries and abundances. *Cell* **163**, 712–723 (2015).
8. L. Ding *et al.*, A genome-scale RNAi screen for Oct4 modulators defines a role of the Paf1 complex for embryonic stem cell identity. *Cell Stem Cell* **4**, 403–415 (2009).
9. L. Wang *et al.*, The THO complex regulates pluripotency gene mRNA export and controls embryonic stem cell self-renewal and somatic cell reprogramming. *Cell Stem Cell* **13**, 676–690 (2013).
10. X. Wang, Y. Chang, Y. Li, X. Zhang, D. W. Goodrich, Thoc1/Hpr1/p84 is essential for early embryonic development in the mouse. *Mol. Cell. Biol.* **26**, 4362–4367 (2006).
11. A. Mancini *et al.*, THOC5/FMIP, an mRNA export TREX complex protein, is essential for hematopoietic primitive cell survival in vivo. *BMC Biol.* **8**, 1–17 (2010).
12. V. O. Wickramasinghe, R. A. Laskey, Control of mammalian gene expression by selective mRNA export. *Nat. Rev. Mol. Cell Biol.* **16**, 431–42 (2015).
13. S. Younis *et al.*, The ZBED6-IGF2 axis has a major effect on growth of skeletal muscle and internal organs in placental mammals. *Proc. Natl. Acad. Sci. U.S.A.* **115**, E2048–E2057 (2018).
14. X. Wang *et al.*, ZBED6 negatively regulates insulin production, neuronal differentiation, and cell aggregation in MIN6 cells. *FASEB J.* **33**, 88–100 (2019).
15. R. Naboulsi, M. Larsson, L. Andersson, S. Younis, ZBED6 regulates Igf2 expression partially through its regulation of miR483 expression. *Sci. Rep.* **11**, 19484 (2021).
16. X. Wang *et al.*, ZBED6 counteracts high-fat diet-induced glucose intolerance by maintaining beta cell area and reducing excess mitochondrial activation. *Diabetologia* **64**, 2292–2305 (2021).
17. S. Younis *et al.*, The importance of the ZBED6-IGF2 axis for metabolic regulation in mouse myoblast cells. *FASEB J.* **34**, 10250–10266 (2020).
18. M. A. Ali *et al.*, Transcriptional modulator ZBED6 affects cell cycle and growth of human colorectal cancer cells. *Proc. Natl. Acad. Sci. U.S.A.* **112**, 7743–7748 (2015).
19. Q. Deng, D. Ramsköld, B. Reinius, R. Sandberg, Single-cell RNA-seq reveals dynamic, random monoallelic gene expression in mammalian cells. *Science* **343**, 193–196 (2014).
20. S. Kanungo, K. Wells, T. Tribett, A. El-Gharbawy, Glycogen metabolism and glycogen storage disorders. *Ann. Transl. Med.* **6**, 474–474 (2018).
21. H. Wakabayashi, M. Tsuchiya, K. Yoshino, K. Kaku, H. Shigei, Hereditary deficiency of lactate dehydrogenase H-subunit. *Intern. Med.* **35**, 550–554 (1996).
22. J. K. Reddy, S. K. Goel, M. R. Nemali, Transcriptional regulation of peroxisomal fatty acyl-CoA oxidase and enoyl-CoA hydratase/3-hydroxyacyl-CoA dehydrogenase in rat liver by peroxisome proliferators. *Proc. Natl. Acad. Sci. U.S.A.* **83**, 1747–1751 (1986).
23. C. Qi *et al.*, Absence of spontaneous peroxisome proliferation in enoyl-CoA hydratase/L-3-hydroxyacyl-CoA dehydrogenase-deficient mouse liver: Further support for the role of fatty acyl CoA oxidase in PPARα ligand metabolism. *J. Biol. Chem.* **274**, 15775–15780 (1999).
24. O. Lieven, J. Knobloch, U. Rüther, The regulation of Dkk1 expression during embryonic development. *Dev. Biol.* **340**, 256–268 (2010).

25. H. Suzuki *et al.*, Structural basis of the autophagy-related LC3/Atg13 LIR complex: Recognition and interaction mechanism. *Structure* **22**, 47–58 (2014).
26. Y. Zhang *et al.*, Dynamic epigenomic landscapes during early lineage specification in mouse embryos. *Nat. Genet.* **501**, 96–105 (2017).
27. K. K. Abe *et al.*, The first murine zygotic transcription is promiscuous and uncoupled from splicing and 3′ processing. *EMBO J.* **34**, 1523–1537 (2015).
28. C. Chen *et al.*, The Vg1-related protein Gdf3 acts in a Nodal signaling pathway in the pre-gastrulation mouse embryo. *Development* **133**, 319–329 (2006).
29. M. T. Johnson, S. Mahmood, M. S. Patel, Intermediary metabolism and energetics during murine early embryogenesis. *J. Biol. Chem.* **278**, 31457–31460 (2003).
30. A. Malkowska, C. Penfold, S. Bergmann, T. E. Boroviak, A hexa-species transcriptome atlas of mammalian embryogenesis delineates metabolic regulation across three different implantation modes. *Nat. Commun.* **13**, 1–12 (2022).
31. A. Fiorenzano *et al.*, Cripto is essential to capture mouse epiblast stem cell and human embryonic stem cell pluripotency. *Nat. Commun.* **7**, 12589 (2016).
32. H. Yan *et al.*, Fatty acid oxidation is required for embryonic stem cell survival during metabolic stress. *EMBO Rep.* **22**, e52122 (2021).
33. R. C. Russell, H. X. Yuan, K. L. Guan, Autophagy regulation by nutrient signaling. *Cell Res.* **24**, 42–57 (2014).
34. U. Kühn, E. Wahle, Structure and function of poly(A) binding proteins. *Biochim. Biophys. Acta* **1678**, 67–84 (2004).
35. G. M. Hautbergue *et al.*, UIF, a new mRNA export adaptor that works together with REF/ALY, requires FACT for recruitment to mRNA. *Curr. Biol.* **19**, 1918–1924 (2009).
36. M. Shi *et al.*, ALYREF mainly binds to the 5′ and the 3′ regions of the mRNA in vivo. *Nucleic Acids Res.* **45**, 9640–9653 (2017).
37. H. Zhang *et al.*, DEAD-box helicase 18 counteracts PRC2 to safeguard ribosomal DNA in pluripotency regulation. *Cell Rep.* **30**, 81–97.e7 (2020).
38. H. R. Ko *et al.*, Roles of ErbB3-binding protein 1 (EBP1) in embryonic development and gene-silencing control. *Proc. Natl. Acad. Sci. U.S.A.* **116**, 24852–24860 (2019).
39. K. M. Neilson *et al.*, Pa2G4 is a novel Six1 co-factor that is required for neural crest and otic development. *Dev. Biol.* **421**, 171–182 (2017).
40. A. Harel *et al.*, Removal of a single pore subcomplex results in vertebrate nuclei devoid of nuclear pores. *Mol. Cell* **11**, 853–864 (2003).
41. T. C. Walther *et al.*, The conserved Nup107-160 complex is critical for nuclear pore complex assembly. *Cell* **113**, 195–206 (2003).
42. A. Ventura *et al.*, Restoration of p53 function leads to tumour regression in vivo. *Nature* **445**, 661–665 (2007).
43. J. Nichols, A. Smith, Naive and primed pluripotent states. *Cell Stem Cell* **4**, 487–492 (2009).
44. C. Bianco *et al.*, Role of Cripto-1 in stem cell maintenance and malignant progression. *Am. J. Pathol.* **177**, 532–540 (2010).
45. W. Zhou *et al.*, HIF1α induced switch from bivalent to exclusively glycolytic metabolism during ESC-to-EpiSC/hESC transition. *EMBO J.* **31**, 2103–2116 (2012).
46. A. L. Goldstein, C. A. Snay, C. V. Heath, C. N. Cole, Pleiotropic nuclear defects associated with a conditional allele of the novel nucleoporin Rat9p/Nup85p. *Mol. Biol. Cell* **7**, 917–934 (1996).
47. M. Smitherman, K. Lee, J. Swanger, R. Kapur, B. E. Clurman, Characterization and targeted disruption of murine Nup50, a p27 Kip1 -interacting component of the nuclear pore complex. *Mol. Cell. Biol.* **20**, 5631–5642 (2000).
48. K. Okita *et al.*, Targeted disruption of the mouse ELYS gene results in embryonic death at peri-implantation development. *Genes Cells* **9**, 1083–1091 (2004).
49. J. Van Deursen, J. Boer, L. Kasper, G. Grosveld, G2 arrest and impaired nucleocytoplasmic transport in mouse embryos lacking the proto-oncogene CAN/Nup214. *EMBO J.* **15**, 5574–5583 (1996).
50. M. E. Dickinson *et al.*, High-throughput discovery of novel developmental phenotypes. *Nature* **537**, 508–514 (2016).
51. Y. Zhang *et al.*, Alterations in cell growth and signaling in ErbB3 binding protein-1 (Ebp1) deficient mice. *BMC Cell Biol.* **9**, 69 (2008).
52. H. Acloque, M. S. Adams, K. Fishwick, M. Bronner-Fraser, M. A. Nieto, Epithelial-mesenchymal transitions: The importance of changing cell state in development and disease. *J. Clin. Invest.* **119**, 1438–1449 (2009).
53. T. Chen, Y. You, H. Jiang, Z. Z. Wang, Epithelial–mesenchymal transition (EMT): A biological process in the development, stem cell differentiation, and tumorigenesis. *J. Cell. Physiol.* **232**, 3261–3272 (2017).
54. E. W. Deutsch *et al.*, The ProteomeXchange consortium at 10 years: 2023 update. *Nucleic Acids Res.* **51**, 1539-1548 (2023).